Magnetization reversal in half metallic $La_{0.7}Sr_{0.3}MnO_3$ films grown onto vicinal surfaces

P. Perna,[1,a)] C. Rodrigo,[1,2] E. Jiménez,[1,2] N. Mikuszeit,[1,2] F. J. Teran,[1] L. Méchin,[3] J. Camarero,[1,2] and R. Miranda[1,2]
[1]*Instituto Madrileño de Estudios Avanzados en Nanociencia IMDEA-Nanociencia, Campus Universidad Autónoma de Madrid, 28049 Madrid, Spain*
[2]*Departamento de Fisica de la Materia Condensada and Instituto "Nicolás Cabrera," Universidad Autónoma de Madrid, 28049 Madrid, Spain*
[3]*GREYC (UMR6072) CNRS-ENSICAEN & Université de Caen Basse-Normandie, Bd. de Marèchal Juin, 14050 Caen, France*

(Presented 15 November 2010; received 1 October 2010; accepted 16 December 2010; published online 23 March 2011)

We present the study of the magnetic properties of well-characterized epitaxial half metallic $La_{0.7}Sr_{0.3}MnO_3$ films grown onto vicinal $SrTiO_3(001)$ substrates with different miscut angles. Room temperature high resolution vectorial Kerr magnetometry measurements have been performed at different applied magnetic field directions in the whole angular range. The films present a substrate-induced uniaxial (twofold) magnetic anisotropy originated from in-plane [110]-oriented elongated structures, whereas the strength of this anisotropy increases with the miscut angle of the substrate surfaces. Our results demonstrate that we can artificially control the magnetic anisotropy of epitaxial films, up to 120 nm thick, by exploiting the substrate-induced anisotropy. We also determine in this case the minimum vicinal angle required to get well-defined uniaxial magnetic anisotropy. © *2011 American Institute of Physics*. [doi:10.1063/1.3560893]

In cubic crystal symmetry epitaxial magnetic thin films the competition between the biaxial (fourfold) and the additional uniaxial (twofold) anisotropies can result in a magnetic reorientation, which depends on many parameters, such as substrate step density,[1,2] thickness,[3] angle of deposition,[4] and even the temperature range.[3] The biaxial and uniaxial anisotropies originate from the crystal symmetry and substrate-induced anisotropy, respectively. By resorting to the fabrication of artificial heterostructures,[5] thin films,[6–8] and superlattices,[9] we can exploit the symmetry breaking in order to control and tailor the magnetic properties of the materials, and, therefore, alter both magnetization easy and hard axes, and reversal processes.[10]

Half metallic $La_{0.7}Sr_{0.3}MnO_3$ (LSMO) manganite, showing both a Curie temperature above 300 K and an almost 100% spin polarization, is of particular interest for the engineering of spintronics devices operating at room temperature (RT) such as read-heads magnetic hard disks and nonvolatile magnetic memories.[11] In this system, the substrate induces tensile or compressive strain to the film depending on the film–substrate lattice mismatch, determining in-plane or out-of-plane easy magnetization directions, respectively.[12] In particular, in LSMO/$SrTiO_3$(STO)(001) an in-plane biaxial magnetic anisotropy ascribed to the substrate-induced in-plane tensile strain is generally observed.[12,13] Moreover, by using vicinal surfaces we can fabricate artificially periodic stepped surfaces with in-plane magnetic anisotropy.[14] In vicinal substrates, the surfaces are intentionally misoriented to a (near) low index surface, therefore determining surface step edges. In such a way, the high symmetry of the low index surface is broken and an additional uniaxial anisotropy is expected.[15] In-plane uniaxial magnetic anisotropy at RT already has been reported in 25- and 7-nm-thick LSMO films deposited on very low miscut STO substrates (0.13° and 0.24°).[3] More recently, some of the authors reported on a well-defined uniaxial magnetic anisotropy in LSMO film, up to 70 nm thick, deposited on 10° vicinal STO(001) substrate.[16]

We have grown 120-nm-thick LSMO thin films by pulsed laser deposition from a stoichiometric target onto commercially available vicinal STO(001) substrates with miscut angle θ_v of 2°, 4°, 8°, 10°. The vicinal angle θ_v was from the [001] surface toward the $[1\bar{1}0]$ crystallographic direction, thus inducing step edges along the [110] direction.[14] The laser fluence was 1–2 J cm^{-2}, the target-to-substrate distance, the oxygen pressure, and the substrate temperature were optimized to 50 mm, 0.35 mbar, and 720 °C, respectively.[9] The crystal structure was investigated by means of x-ray diffraction (XRD). The XRD θ–2θ -scans indicate that the LSMO films were epitaxially grown on the substrates. In particular, the LSMO films present the (001) axis parallel to the (001) axis of the substrate. The out-of-plane and the in-plane lattice parameters were determined by XRD measurements around symmetric and asymmetric crystallographic peaks. For all films, the measured lattice parameters and the strain tensor components along the [100] ($\epsilon_{[100]}$) in-plane crystallographic direction present the two in-plane lattice parameters of the LSMO cell equally tensile strained ($\epsilon_{[100]} = \epsilon_{[010]} < 1.0\%$) by the substrate. The crystalline quality of the films was checked by measuring the full width at half maximum of the rocking curves (ω scan),

a)Author to whom correspondence should be addressed. Electronic mail: paolo.perna@imdea.org.

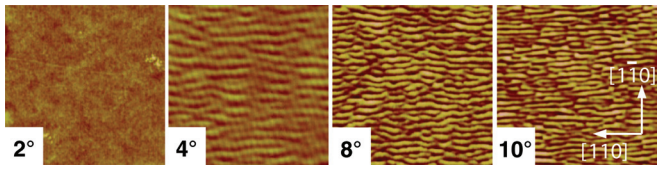

FIG. 1. (Color online) $1 \times 1\ \mu m^2$ AFM images of the LSMO films grown onto 2°, 4°, 8°, and 10° miscut STO substrates. Clear elongated structures on the top surface, oriented along the [110] crystallographic direction, are found in 4°, 8°, and 10° miscut samples. No clear structures are observed in the lowest miscut film, i.e., 2°.

which are always found below 0.15°, and the in-plane crystal plane alignment (ϕ scan). It is worth noting that in all the investigated samples, the Curie temperature was always found above RT.[14]

The morphology of the samples was investigated at RT by means of atomic force (AFM) and scanning tunnel microscopies, using a Nanoscope microscope. The average roughness (rms) of the samples was found always in the range of few unit cells. In general, the morphology of the LSMO films replicates that of the substrates. In particular, as demonstrated by the 1 μm × 1 μm AFM measurements reported in Fig. 1, the LSMO films grown onto 4°, 8°, and 10° miscut substrates present elongated structures on the top surface oriented along the [1$\bar{1}$0] crystallographic direction, i.e., parallel to the substrate step edges. The LSMO film grown onto low miscut STO substrate, i.e., $\theta_v = 2°$, present smoother and flatter surface and no clear elongated structures are observed.

The magnetic properties, including magnetization reversal and magnetic anisotropy, of the films was studied at RT by high-resolution vectorial-Kerr magnetometry measurements using *p*-polarized incident light. We measured simultaneously the in-plane vectorial-resolved hysteresis loops, i.e., $M_{||}(H,\theta)$ and $M_{\perp}(H,\theta)$, as a function of the sample in-plane angular rotation angle (θ), keeping fixed the external magnetic field direction.[17] The whole angular range was probed every 4.5°, with 0.5° angular resolution.

Figure 2 shows representative Kerr hysteresis loops of 120-nm-thick LSMO films grown onto 2° and 8° miscut STO(001) acquired at $\theta = 0°$ and $\approx 90°$, where $\theta = 0°$ is taken when the external field is aligned parallel to the [110] in-plane crystal direction, i.e., parallel to the substrate step

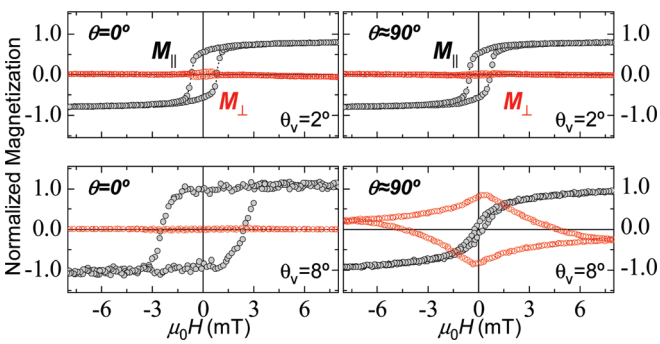

FIG. 2. (Color online) Representative hysteresis loops of the parallel [perpendicular] components of the magnetization $M_{||}(H)$ [$M_{\perp}(H)$] acquired at $\theta = 0°$ (closed symbol) and $\theta \approx 90°$ (open) directions of 120-nm-thick LSMO films grown onto 2° (top panels) and 8° (bottom panels) miscut STO(001) substrates. $\theta = 0°$ is taken when the external field is aligned parallel to the [110] in-plane crystal direction, i.e., parallel to the substrate step direction.

direction. For the LSMO film grown on the lowest miscut STO substrate, i.e., $\theta_v = 2°$, the $M-H$ loops present very small changes when comparing the behavior at $\theta = 0°$ and 90°. $M_{||}(H)$ loops show mainly a sharp (irreversible) transition and negligible $M_{\perp}(H)$ loops (Fig. 2 top panels). This is the expected behavior of easy-axis directions of magnetization. Supporting this, $M_{\perp}(H)$ changes the sign when the e.a. direction is crossed (not shown). In turn, smooth reversible transitions become more relevant during reversal approaching $\theta =$ e.a. $\pm 45°$, where $M_{\perp}$ signals are maximum, i.e., hard-axis (h.a.) directions. These features reflect the fourfold symmetry of the magnetic anisotropy. In clear contrast, the LSMO films grown onto higher miscut substrates present twofold magnetic anisotropy (Fig. 2 bottom panels). The $M-H$ loops show characteristic e.a. and h.a. behaviors at $\theta = 0°$ and $\theta \approx 90°$, respectively. The e.a. (h.a.) direction is parallel (perpendicular) to the elongated structures.

Regarding the magnetization reversal processes, the $M-H$ loops of Fig. 2 reveal that sharp (irreversible) transitions dominate the reversal at the e.a. direction, whereas smooth (reversible) transitions dominate at the h.a. direction. As expected for extended systems, this indicates that magnetization reversal mainly proceeds by nucleation and further propagation of magnetic domains and by rotation processes, respectively. This picture has been strongly supported recently in real space by means of angular dependent Kerr microscopy measurements in 10° miscut LSMO films.[16]

The symmetry of the magnetic anisotropy for the different films is more clear when the angular dependence of the normalized remanence of both magnetization components, i.e., $M_{||,R}/M_S$ and $M_{\perp,R}/M_S$, is plotted [Figs. 3(a) and 3(b)]. In all cases, both magnetization components show a pronounced oscillation with periodicity of 180°. However, in the lowest miscut sample, i.e., $\theta_v = 2°$, an additional 90° periodicity is found. In particular, $M_{||,R}$ presents two maxima (minima) which correspond to two orthogonal e.a. at 0° and 90° (h.a. at 45° and 135°), indicating a fourfold magnetic anisotropy (Fig. 3 top panels). It is worth noting that the two maxima show different values at the e.a., and the maximum value coincides with the substrate surface steps direction. This is signature of the existence of two anisotropies, i.e., biaxial and uniaxial, originated from the cubic crystal symmetry and the step-induced anisotropy, respectively. In clear contrast, for high miscut LSMO films, i.e., $\theta_v = 4°$ to 10°, the $M_{||,R}$ follows a perfect $|\cos\theta|$ law dependence, whereas the $M_{\perp,R}$ changes the sign when a characteristic direction, i.e., e.a. and h.a. directions, is crossed (Fig. 3 bottom panels). In addition, $M_{||,R} = 0$ at the h.a., which is a typical feature of well-defined uniaxial anisotropy systems. The magnetic anisotropy is clearly visualized in the polar plot of the parallel component of the remanence magnetization (insets of Fig. 3). In the case of lowest miscut film $M_{||,R}$ presents a "4-leaves clover"-like behavior, signature of a biaxial anisotropy, whereas in the case of high miscut LSMO films, the well-defined uniaxial anisotropy is highlighted by the "two-lobe" behavior of the $M_{||,R}$. This indicates a magnetic anisotropy transition as θ_v increases, which can be ascribed to the competition between the magnetocrystalline (fourfold) anisotropy and the substrate-induced (twofold) anisotropy.

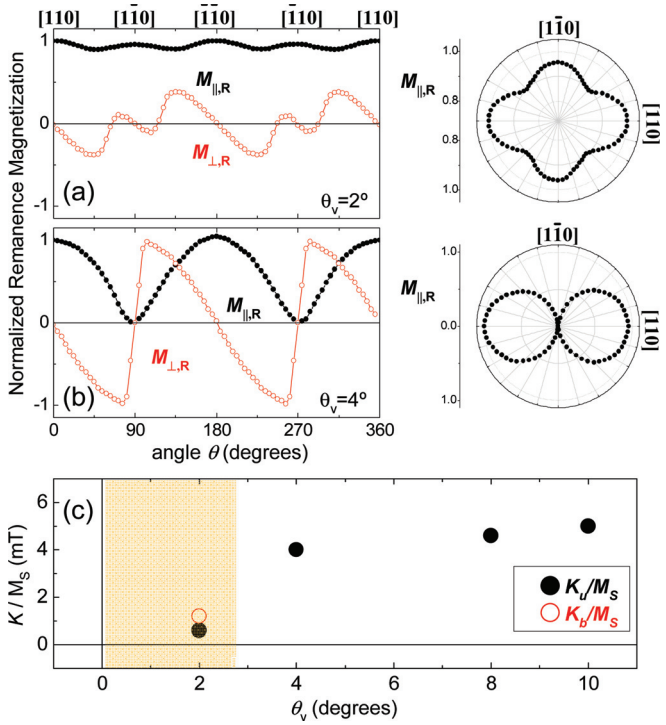

FIG. 3. (Color online) Angular dependence of the normalized remanence magnetization ($M_{||,R}/M_S$ and $M_{\perp,R}/M_S$) of 120-nm-thick LSMO films grown onto a vicinal (a) $\theta_v = 2°$ and (b) 4° STO(001) surfaces. The right panels show the corresponding polar-plot representations of $M_{||,R}$. Note that different scale is adopted for the 2° miscut film. (c) Miscut angle θ_v dependence of uniaxial anisotropy K_u (closed symbols) and biaxial anisotropy K_b (open symbols) constants. The shadowed area highlights the region of non-negligible biaxial anisotropy.

In order to discuss the dependence of the substrate vicinality on the magnetic anisotropy strength of the 120-nm-thick LSMO films, we have plotted in Fig. 3(c) the anisotropy constants normalized to the magnetization saturation (M_S) vs miscut angle (θ_v). The twofold uniaxial anisotropy K_u and the fourfold biaxial anisotropy K_b constants, as defined in Ref. 14, are calculated from anisotropy field ($\mu_0 H_K$) values. The latter is extracted from fitting to the h.a. hysteresis loops. In accordance with the above-presented discussion, two collinear anisotropy contributions, fourfold and twofold symmetry, have been considered for the LSMO film grown onto the lowest vicinal angle investigated, i.e., $\theta_v = 2°$, whereas just an uniaxial anisotropy contribution ($K_b = 0$) has been used for the rest of the films, $\theta_v > 4°$. In turn, K_u gives a more direct view of the anisotropy strength of the films and also increases when θ_v increases. This could be directly related with the topography of the films, because a larger density of elongated structures (i.e., larger aspect ratio) is found in the LSMO films grown on higher vicinality STO substrates, as Fig. 1 shows. A more quantitative analysis, including LSMO films with different thicknesses and θ_v, is needed in order to confirm this trend as well as the onset of the substrate vicinal cut for which the uniaxial anisotropy dominates. In the present study, the data show that the strength of the uniaxial anisotropy increases as θ_v increases.

In conclusion, we have engineered the growth of half metallic epitaxial LSMO films in order to obtain purpose-designed magnetic anisotropy exploiting the anisotropy induced by vicinal substrates with different miscut angles. To do so, we have investigated the effects of the vicinal surfaces on the magnetic properties of LSMO films by high-resolution vectorial Kerr magnetometry. The dominance of the uniaxial anisotropy over the biaxial anisotropy is achieved in 120-nm-thick LSMO films grown onto high miscut vicinal STO(001) susbtrates. Keeping fixed the film thickness, the surface-induced anisotropy determines well-defined uniaxial magnetic anisotropy for vicinal surfaces with miscut angle higher than 4°, with the e.a. lying along the direction of surface step edges. For lower miscut LSMO films, fourfold magnetic anisotropy features are found. We have shown the angular dependence of the magnetization reversal processes from the detailed analysis of the vectorial-resolved Kerr loops. In this work, we have demonstrated the ability to control and tailor the magnetic properties of 120-nm-thick LSMO films by exploiting vicinal surfaces. This is an important task for the design of devices based on thin film technology.

ACKNOWLEDGMENTS

This work was supported in part by the Spanish MICINN through Project No. CSD2007-00010 and by the Comunidad de Madrid through Project No. S2009/MAT-1726. P.P. thanks the European Science Foundation (ESF) through the activity entitled "Thin Films for Novel Oxide Devices" (http://www.ims.tnw.utwente.nl/thiox/) for partial financial support through exchange grants.

[1] A. Berger, U. Linke, and H. P. Oepen, Phys. Rev. Lett. **68**, 839 (1992).
[2] A. Stupakiewicz, A. Kirilyuk, A. Fleurence, R. Gieniusz, T. Maroutian, P. Beauvillain, A. Maziewski, and Th. Rasing, Phys. Rev. B **80**, 094423 (2009).
[3] M. Mathews, F. M. Postma, J. C. Lodder, R. Jansen, G. Rijnders, and D. H. Blank, Appl. Phys. Lett. **87**, 242507 (2005).
[4] S. van Dijken, G. Di Santo, and B. Poelsema, Phys. Rev. B **63**, 104431 (2001).
[5] J. J. de Miguel and R. Miranda, J. Phys. Condens. Matter **14**, R1063 (2002).
[6] M. J. Zhuo, Y. L. Zhu, X. L. Ma, and H. B. Lu, Appl. Phys. Lett. **88**, 071905 (2006).
[7] T. Taniuchi, H. Kumigashira, M. Oshima, T. Wakita, T. Yokoya, M. Kubota, K. Ono, H. Akinaga, M. Lippmaa, M. Kawasaki, and H. Koinuma, Appl. Phys. Lett. **89**, 112505 (2006).
[8] A. Ruotolo, A. Oropallo, F. Miletto Granozio, P. Perna, and U. Scotti di Uccio, Appl. Phys. Lett. **88**, 252504 (2006); A. Ruotolo, A. Oropallo, F. Miletto Granozio, G. P. Pepe, P. Perna, U. Scotti di Uccio, and D. Pullini, *ibid.* **91**, 132502 (2007).
[9] P. Perna, L. Méchin, M. P. Chauvat, P. Ruterana, Ch. Simon, and U. Scotti di Uccio, J. Phys. Condens. Matter **21**, 306005 (2009).
[10] D. Ecija, E. Jiménez, N. Mikuszeit, N. Sacristán, J. Camarero, J. M. Gallego, J. Vogel, and R. Miranda, Phys. Rev. B **77**, 024426 (2008); D. Ecija, E. Jiménez, N. Mikuszeit, N. Sacristán, J. Camarero, J. M. Gallego, J. Vogel, and R. Miranda, J. Magn. Magn. Mater. **316**, 321 (2007).
[11] J.-H. Park, E. Vescovo, H.-J. Kim, C. Kwon, R. Ramesh, and T. Venkatesan, Nature (London) **392**, 794 (1998).
[12] F. Tsui, M. C. Smoak, T. K. Nath, and C. B. Eom, Appl. Phys. Lett. **76**, 2421 (2000).
[13] M. Ziese, H. C. Semmelhack, and P. Busch, J. Magn. Magn. Mater. **246**, 327 (2002).
[14] P. Perna, C. Rodrigo, E. Jiménez, F. J. Teran, N. Mikuszeit, L. Méchin, J. Camarero, and R. Miranda, http://arxiv.org/abs/1005.0553.
[15] R. A. Hyman, A. Zangwill, and M. D. Stiles, Phys. Rev. B **58**, 9276 (1998).
[16] P. Perna, L. Méchin, M. Saïb, J. Camarero, and S. Flament, New J. Phys. **12**, 103033 (2010).
[17] J. Camarero, J. Sort, A. Hoffmann, J. M. García-Martín, B. Dieny, R. Miranda, and J. Nogués, Phys. Rev. Lett. **95**, 057204 (2005).